PCCP

Accepted Manuscript

ROYAL SOCIETY OF CHEMISTRY

www.rsc.org/pccp

GRAPHICAL ABSTRACT

Influence of Applied Silica Nanoparticles on Bio-renewable Castor Oil Based Polyurethane Nanocomposite and its Physicochemical Properties

Kamal Mohamed Seeni Meera,[a] Rajavelu Murali Sankar,[a] Jaya Paul,[a] Sellamuthu N Jaisankar,[a] and Asit Baran Mandal,[*ab]

[a]*Polymer Division, Council of Scientific and Industrial Research (CSIR) – Central Leather Research Institute (CLRI), Adyar, Chennai 600020, Tamil Nadu, India.*
[b]*Chemical Laboratory, Council of Scientific and Industrial Research (CSIR) – Central Leather Research Institute (CLRI), Adyar, Chennai 600020, Tamil Nadu, India.*
E-mail: abmandal@hotmail.com; abmandal@clri.res.in
Tel.: +91-44-24910846/0897; Fax: +91-44-24912150/1589.

Bio-renewable castor oil polyurethane/silica nanocomposite films made, which improved thermal, surface and mechanical properties. These films find application in biomaterials development.

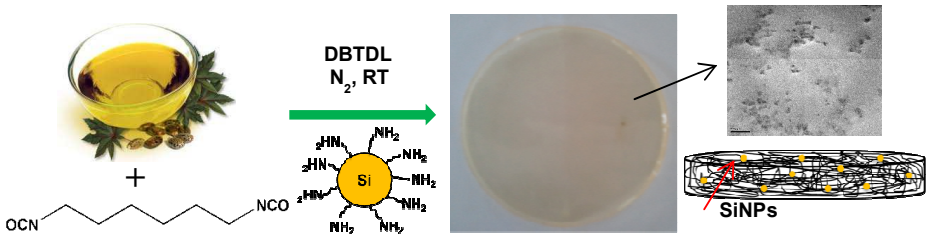

Cite this: DOI: 10.1039/c0xx00000x

www.rsc.org/xxxxxx

PAPER

Influence of Applied Silica Nanoparticles on Bio-renewable Castor Oil Based Polyurethane Nanocomposite and its Physicochemical Properties†

Kamal Mohamed Seeni Meera,[a] Rajavelu Murali Sankar,[a] Jaya Paul,[a] Sellamuthu N Jaisankar,[a] and Asit Baran Mandal,[*a,b]

Received (in XXX, XXX) Xth XXXXXXXXX 20XX, Accepted Xth XXXXXXXXX 20XX
DOI: 10.1039/b000000x

Novel bio-renewable castor oil based polyurethane (PU)/silica nanocomposite films were prepared using castor oil, 1,6-hexamethylene diisocyanate and dibutyltin dilaurate in tetrahydrofuran at room temperature. ATR-FTIR spectra confirm the formation of polyurethane and presence of silica nanoparticles in the polyurethane matrix. The increase of Si nanoparticle content shift the peak position of N-H and C=O (both hydrogen and non-hydrogen bonded) groups present in the polyurethane structure. Furthermore, Raman spectra confirmed the urethane-amide interaction present in the polyurethane/silica nanocomposites. ^{29}Si CP/MAS NMR spectra evidence the formation and presence of completely condensed SiO_2 species in the polyurethane nanocomposite films. The incorporation of silica nanoparticle increases the thermal stability of the above polyurethane films, which can be seen from the increase in activation energy (E_a) values of the degradation process. The E_a values at two stages (T_{max1} and T_{max2}) of degradation process are 133, 139 and 157, 166 kJ/mol for PU control and PU-5AMS (5 wt % amine modified silica nanoparticles), respectively. DSC results prove the interfacial interaction present between silica nanoparticles and polyurethane hard segment, which decreases the melting temperature. Optical transmittance of the polyurethane films decreased with increasing silica content due to the scattering at the interfaces between the silica nanoparticles and polyurethane. It is interesting to note that the presence of silica nanoparticles giving reinforcement to polyurethane film thereby increasing the storage modulus up to 24% for PU-5AMS. FE-SEM and HR-TEM images confirm the presence of silica nanoparticle in polyurethane matrix.

1. Introduction

Over the years tremendous efforts have been made to combine the properties of polymer matrix (organic part) and nanoscale building blocks (inorganic part) to achieve improved functional properties over conventional organic polymer matrix.[1] These nanocomposite materials exhibit good adhesion between the polymer matrix and nano fillers because of the nano size, higher surface area and surface-to-volume ratio of the nanoscale building blocks.[2] The introduction of smaller amount of nano filler can provide higher thermal, mechanical, optical, flame retardancy and gas transport properties.[3] The most frequently used nano fillers are montmorillonite (MMT) clay, silica (Si) nanoparticles, carbon nanotubes, graphene, etc.[4-7]Among them, silica nanoparticles (SiNPs) has been received much attentions due its mild synthetic preparative conditions, large surface area, smooth nanoporous surface, high adsorption capacity, large pore volume, etc.[8] Moreover, the incorporation of silica nanoparticles into the polymer matrix increases the performance of polymers and impart some novel properties to the polymer matrix. In the recent past, it has been described that the most versatile method to prepare silica nanoparticle is 'sol-gel' approach, which has an added advantages of processing the nanocomposites at relatively low temperature and utilizes very mild synthetic conditions.[9,10] In order to improve and enhance the dispersion, surface activity and stability of the silica nanoparticles, the surface of SiNPs modified with silane surface modifiers. The commonly used modifiers are 3-aminopropyltrimethoxysilane, 3-aminopropyltriethoxysilane, methacryloxypropyltriethoxysilane, etc. The surface modification of SiNPs will provide better compatibility between the nanoparticles and polymer matrix and further, which prevents the agglomeration of nanoparticles.[11]

There are several polymer systems used for the preparation of polymer/silica nanocomposites. Of which, polyurethane (PU) has

[a]*Polymer Division, Council of Scientific and Industrial Research (CSIR) – Central Leather Research Institute (CLRI), Adyar, Chennai 600020, Tamil Nadu, India.*
[b]*Chemical Laboratory, Council of Scientific and Industrial Research (CSIR) – Central Leather Research Institute (CLRI), Adyar, Chennai 600020, Tamil Nadu, India.*
E-mail: abmandal@hotmail.com; abmandal@clri.res.in
Tel.: +91-44-24910846/0897; Fax: +91-44-24912150/1589.
† Electronic Supplementary Information (ESI) available: [FT-IR, GPC, TGA, tensile, SEM and XPS data]. See DOI: 10.1039/b000000x/

received much importance due to its range of physicochemical properties and variety of applications.[12,13] The main advantage of having polyurethane is the achievement of tailored made properties like flexibility, elasticity and damping ability by altering the molecular chain structure.[14] Polyurethanes have wide range of applications in the field of coatings, adhesives, fibers, foams, reaction molding plastics, biomaterials, etc.[15,16] However, the main drawbacks associated with the use of petroleum resources for the preparation and development of polyurethanes are environmental pollution, waste disposal, high price, depletion of petroleum raw materials, etc.[17,18] Therefore, researchers are focusing towards the use of non-polluting and easily available bio-renewable resources for preparing these kinds of polymeric materials with good performance at competitively low price. Bio-renewable resources based on vegetable and plant oils are most often replacing the use of petroleum products in industry.[19] Among various oils, castor oil is an important triglyceride having the combination of hydroxyl group and unsaturation in the fatty acid chain uniquely. The presence of hydroxyl functionality is one of the major advantages of castor oil, which can easily react with isocyanates to give polyurethanes, interpenetrating polymer networks, elastomers, coatings, hyper branched polymers, foams, etc.[20] Very recently, we have demonstrated and reported castor oil based polyurethane/siloxane cross-linked film structures for hydrophobic surface coatings with improved thermal, mechanical and optical properties.[21] Castor oil based polyurethanes reported to have antibacterial activity and could be used for wound dressing applications.[22] Sharmin *et al.*[23] reported that castor oil based bio-hybrid could be used as nanostructured protective coatings up to 180 °C. Castor oil polyurethane-urea/silica hybrid may be used for the development of high performance materials and coatings.[24]

In view of the above merits, we have chosen castor oil as a starting material for preparing the polyurethane and combined the advantages of silica nanoparticle to get new polymeric material with improved properties. The main goal of the present work is to develop bio-renewable castor oil based polyurethane/silica nanocomposite films at room temperature with good thermal, surface, and mechanical properties. Initially, castor oil polyurethanes were made at room temperature by reacting castor oil with 1,6-hexamethylene diisocyanate in tetrahydrofuran medium using a dibutyltin dilaurate catalyst at very low concentration. To this prepared polyurethane solution, various concentrations of silica nanoparticles were added and cast on a mold to get uniform films. The obtained nanocomposite films were characterized in understanding their structural, thermal, surface, mechanical and morphological properties using various physicochemical techniques in order to exploit its physicochemical aspects.

2. Experimental section

2.1 Materials

Castor oil (mol. formula: $C_{57}H_{104}O_9$, hydroxyl number: 164 mg KOH/g, mol. wt.: 932) was purchased from Bison Laboratories, India. The moisture present in castor oil was removed by heating at 80 °C for 4 h under vacuum. The hexamethylene diisocyanate (HDI), tetraethylorthosilicate (TEOS), 3-aminopropyltrimethoxysilane (APTMS) were purchased from Sigma Aldrich, USA, and used as received. Dibutyltin dilaurate (DBTDL) was purchased from Fluka, USA. Ammonia solution, absolute ethanol and tetrahydrofuran (THF) were received from Merck, India, and used after distillation. Double distilled water of specific conductance 2-3 μScm^{-1} at 25 °C was used throughout the experiments.

2.2 Preparation of amine modified silica nanoparticles (AMS)

The AMS were prepared according to the following procedure reported elsewhere.[25] 50 mL of absolute ethanol and 3.4 mL of ammonia solution were mixed in a 100 mL round bottom flask equipped with magnetic stirrer at room temperature (RT). Then 3.5 mL of tetraethylorthosilicate was added to it drop wise and the mixture were allowed for stirring at RT for 24 h. After that, 0.7 mL of 3-aminopropyltrimethoxysilane was added drop wise to it under RT (25 °C) and continued for another 24 h. Further, the solution washed with absolute ethanol for several times and centrifuged. The particle size [Z-Average (in radius)] was found to be 75.2 and 84.2 nm for unmodified (UMS) and amine modified (AMS) silica nanoparticles, respectively. The chemical modification of silica nanoparticle surface with amino group was confirmed using FT-IR spectra (see Fig. S1, ESI).

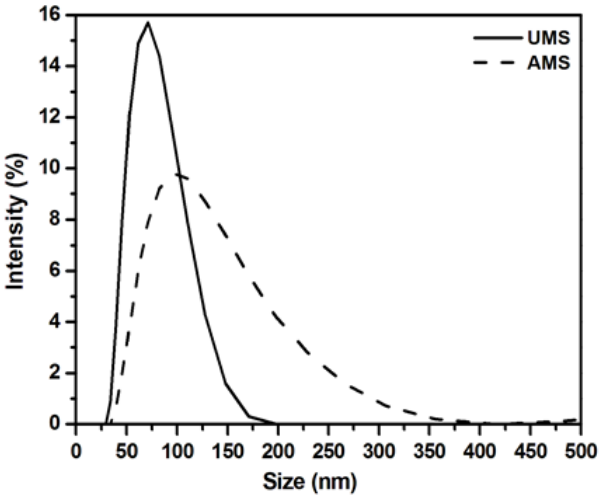

Fig. 1 Particle size distribution of prepared silica nanoparticles.

The particle size distribution (PSD) plot for the prepared silica nanoparticles were given in Fig. 1. It can be seen from the PSD plot that modification of silica surface with amino group resulted in increase of particle size from 75.2 (UMS) to 84.2 nm (AMS). Similar kind of increase in particle size value reported for Si nanoparticles modified with different amino silane coupling agents.[26] The presence of NH_2 group induces particle growth, which increases the rate of hydrolysis and produces bigger size particles with broader distribution.[26] The SEM images of UMS and AMS were given in Fig. S2, which proves that the silica nanoparticles are uniform in size and spherical shape.

2.3 Preparation of castor oil PU/silica nanocomposite

The preparation of PU/silica nanocomposite consists of two-step process. In the first step, castor oil polyurethane was synthesized in a three-necked round bottom flask equipped with a magnetic stirrer, nitrogen (N_2) flow inlet and an addition funnel for adding diisocyanate and solvent. Initially, castor oil was

heated at 80 °C for 4 h to remove the moisture content. This castor oil was taken in a 100 mL three-necked round bottom flask and stirred in THF to get uniform solution under N_2 atmosphere. To this solution, calculated amount of hexamethylene diisocyanate was added drop wise and a drop of 0.001% of DBTDL catalyst was also added to it. Then the solution was allowed for stirring at room temperature for 4 h. After 4 h of reaction (Scheme 1), different wt % of amine modified silica nanoparticles were added (step 2). The stirring was continued further for another 15 min to get a uniform solution and then cast into a petri-dish to obtain as films. The codes and chemical compositions of the polyurethane/silica nanocomposite films were given in Table 1. The number average molecular weight (M_n) of the prepared castor oil polyurethane is 9131 and the respective GPC trace given in Fig. S3.

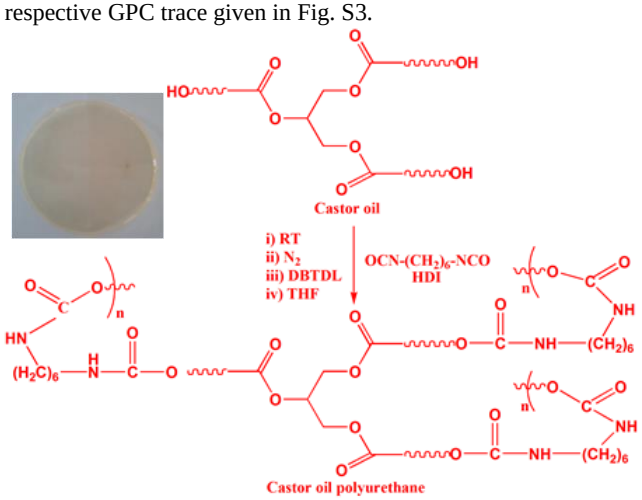

Scheme 1 Preparation of castor oil PU (Inset: photograph of PU films).

Table 1 Codes and chemical compositions for PU/silica nanocomposites.

Codes	Compositions			
	NCO:OH ratio	DBTDL (%)	UMS (wt %)	AMS (wt %)
PU control	3:1	0.001	-	-
PU-1UMS			1	-
PU-0.5AMS			-	0.5
PU-1AMS			-	1.0
PU-3AMS			-	3.0
PU-5AMS			-	5.0

2.4 Characterization of polyurethane/silica nanocomposites

The infrared spectra of the nanocomposite film samples were recorded using ABB MB3000 Fourier-transform infrared spectrometer in ATR mode by keeping the films over ZnSe crystal with a resolution of 16 cm^{-1} over a scans of 60. Raman spectra of the nanocomposite films were recorded using Raman spectrometer (Witch confocal Raman microscopy alpha 300 R). The particle size measurements were done using a Zetasizer 3000 HS_A equipped with a digital auto-correlator from Malvern Instrument, UK. The molecular weight of the prepared polyurethane recorded on a WATERS GPC, TA Instruments, USA, and THF solvent was used as an eluent with a flow of 1 mL/min. The ^{29}Si solid state NMR spectra of the nanocomposite films were recorded using Bruker Avance 400 MHz NMR spectrometer, Germany, at a frequency of 79.49 MHz with cross-polarization magic-angle-spinning (CP/MAS) technique. The thermogravimetric analyses were performed using TG Analyzer-Model Q50, TA Instruments, USA, under N_2 atmosphere with a flow rate of 40-60 mL/min with different heating rates ranging 5, 10, 15 and 20 °C/min. Samples of around 10 mg was heated from 30 to 800 °C. Differential scanning calorimetric analyses were performed using DSC-Model Q200, TA Instruments, USA, by heating the samples of around 3-5 mg from -90 to 300 °C at a heating rate of 10 °C/min with a N_2 flow of 50 mL/min. Contact angle measurements were taken on contact angle meter from Holmarc Opto Mechatronics Pvt Ltd., India. Static contact angle of water and hexadecane (drop of 10 µL) were measured and surface free energy was calculated using the standard Owens and Wendt[47] equation. UV-visible transmittance spectra were recorded on Cary 50 Bio UV-vis spectrophotometer from Varian. Dynamic mechanical analysis was done using a dynamic mechanical analyzer Q800, TA Instruments, USA, with a constant frequency of 1 Hz along with a load of 0.1 N. The analysis was performed over a temperature range of -100 to 200 °C with a heating rate of 4°C/min. The tensile strength and percentage elongation at break were measured using a universal testing machine (UTM), (Instron 3369, USA) at a cross-head speed of 50 mm/min with 0.30 mm of thickness for all the samples, as per the ASTM D638 test procedure method at 20 °C with a relative humidity of 65%. The mechanical data reported are the averages of five measurements for each sample. The morphology of the polyurethane/silica nanocomposite films was taken using field emission scanning electron microscopy (FE-SEM SU6600, Hitachi). HR-TEM images were taken using transmission electron microscope (FEI Tecnai G2, Germany). XPS analysis of the nanocomposite films was done using X-ray photoelectron spectroscopy (XPS), Omicron Nano Technology, GmbH.

3. Results and discussion

3.1 ATR-FTIR spectra

ATR-FTIR spectra for the polyurethane/silica nanocomposite films were presented in Fig. 2. The formation of polyurethane was confirmed from the disappearance of characteristic –NCO peak at 2270 cm^{-1} in the IR spectra of all polyurethane films. Furthermore, the bands centred at approximately 1742 cm^{-1} was assigned to the stretching vibration of carbonyl region of urethane moiety. The appearance of broad absorption peak centred at 3330 cm^{-1} is attributed to the stretching vibration of –NH of urethane moiety. The above peak shifts to a higher wavenumber with an increase of silica nanoparticles content (PU-1UMS: 3331, PU-0.5AMS: 3332, PU-1AMS: 3334, PU-3AMS: 3336 and PU-5AMS: 3338 cm^{-1}; see Table S1, ESI). The increase in the wave number of –NH region of PU is mainly due to the presence of silica nanoparticles, which strongly interacted with polyurethane moiety, thereby shifting the peak position of –NH groups (Fig. S4a). The shift in the N-H peak position is also due to the cross-linking or hydrogen bonding present in the polyurethane nanocomposite films.[27] Furthermore, the hydrogen bonded and non-hydrogen bonded C=O groups present in the nanocomposite films were monitored and presented in Fig. S4b. It can be seen from the fig. S4b that increasing silica nanoparticle content shift the peak position of C=O group (see Table S1, ESI).[28] The increase in the intensity and peak positions of interacted –N-H and C=O groups clearly indicate the formation of complete and

uniform network structure of PU.[28b] The peaks appeared in the range of 3010-2855 cm^{-1} corresponds to the alkyl region of castor oil and C-H bending was observed at 1374 cm^{-1}. In the cases of AMS incorporated nanocomposites, there may be a chance of formation of urea linkage from NH_2 groups present in the surface of SiNPs with free -NCO of polyurethane. The characteristic peak of silica nanoparticles was observed at around 774 cm^{-1} (O-Si-O) and a strong peak near 1096 cm^{-1} is assigned to Si–O–Si asymmetric stretching vibrations. This confirms the presence of silica nanoparticles in the castor oil polyurethane matrix and forms the nanocomposites.

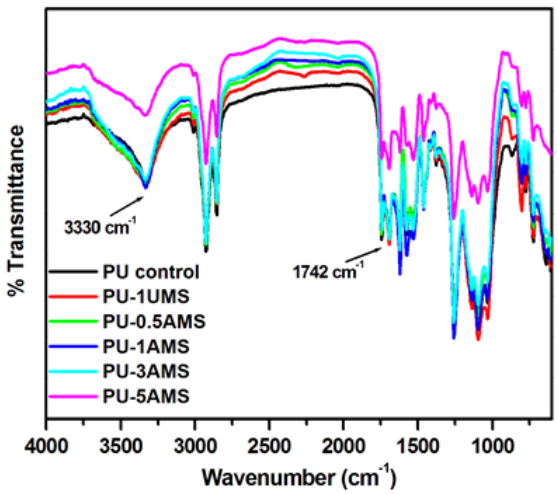

Fig. 2 ATR-FTIR spectra of polyurethane/silica nanocomposite film.

3.2 Raman studies

Raman spectra of control and nanocomposite polyurethane show significant changes in the spectra on increasing the silica nanoparticle concentration in the polyurethane matrix. The control PU shows the characteristic peak at 1304 cm^{-1} assigned to the C-O stretching. Further, peak at 1436 cm^{-1} corresponds to the aliphatic CH_2 stretch and the peak at 1654 cm^{-1} corresponds to the amide moiety of urethane linkage in PU matrix.[29,30] Furthermore, two peaks at 2910 and 2854 cm^{-1} were assigned to the C-H stretching vibration of aliphatic chain present in the castor oil moiety and also be due to protonated amine stretched deformation vibration. The peak at around 1100 cm^{-1} in nanocomposite samples assigned to the Si-O-Si framework vibrations from silica nanoparticle. On subsequent increase in concentration of silica nanoparticles in the PU matrix shows a plateau at 1654 cm^{-1} in Raman spectra (Fig. 3), which may be due the physical interaction of –OH and $–NH_2$ groups present in the SiNPs with polyurethane.[31] From the magnified image of Raman spectra at the region of 1600-1700 cm^{-1} given in Fig. 3, we were able to observe that the intensity of urethane amide peak at 1654 cm^{-1} increases on increasing the concentration of modified silica nanoparticles (AMS) in the nanocomposites (PU-1AMS, PU-3AMS & PU-5AMS). This is due to the presence of well dispersed Si nanoparticles in the PU matrix, which effectively interact with the urethane amide of PU. The Raman peak intensity at 1654 cm^{-1} increased from 1 to 3 wt % of AMS. In the case of 5 wt % of AMS, the peak intensity slightly decreased, which may be due to the formation slight aggregation. However, the unmodified silica nanocomposites (PU-1UMS) show less increase in the intensity of urethane amide peak, which exhibits the lower interaction of nanoparticles in the PU matrix. This finding from Raman analysis helps in confirming the presence of Si nanoparticles and their interaction with PU polymer through urethane-amide moiety. We observed similar kind of urethane amide interaction in the case of polyurethane/carbon nanotube nanocomposite films.[6c]

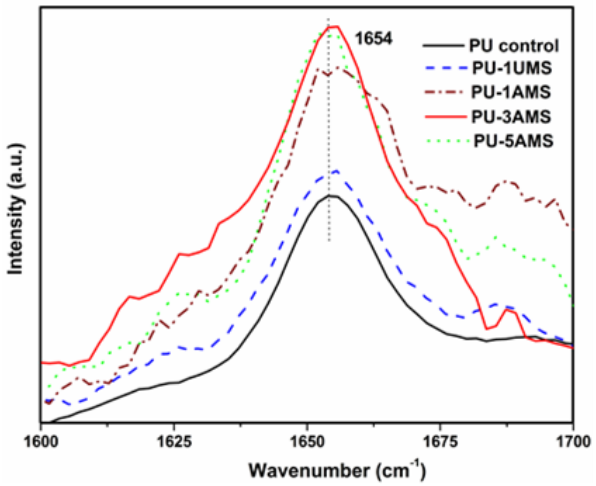

Fig. 3 Expanded regions (1600-1700 cm-1) of Raman spectra for the prepared nanocomposites.

3.3 ^{29}Si solid state NMR spectra

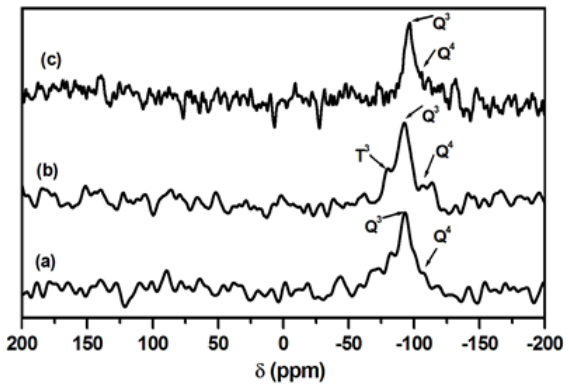

Fig. 4 ^{29}Si solid state CP/MAS NMR spectra of (a) UMS, (b) AMS and (c) PU-1UMS.

The prepared silica nanoparticles and nanocomposite films were analyzed using ^{29}Si solid state CP/MAS NMR to understand the formation of SiNPs and influence of silica on polyurethane and their corresponding spectra given in Figs. 4 & 5. The unmodified silica nanoparticle gives two chemical shifts at -95 and -106 ppm correspond to Q^3 and Q^4 environment (Fig. 4a). The presence of Q^4 peak confirms the presence of completely condensed SiO_2 species and Q^3 peak confirms the presence of silanol (Si-OH) groups on the surface of unmodified silica nanoparticles.[32] In the case of modified silica nanoparticle (Fig. 4b), three chemical shifts were observed at -94 and -105 ppm representing Q^3 and Q^4 environments and T^3 peak appears at -72 ppm. The appearance of T^3 peak confirms the presence of non-hydrolyzed species on the surface of the silica nanoparticles (i.e., 3-aminopropyl moiety).[33] Fig. 5 shows the ^{29}Si NMR spectra of the nanocomposite films, which confirms the presence of silica nanoparticle in the

polyurethane matrix. All the nanocomposite samples show a strong intense peak at -108 ppm corresponds to the Q^4 moiety of completely condensed silica particles. The existence of intensive signals in the range of -60 to -110 ppm evidence the presence of silica nanoparticle. This is in accordance with the increase in concentration of silica nanoparticle (Fig. 5a-d). The increase in Q^4 peak proportion is mainly due to the increasing amount of silica nanoparticle content.

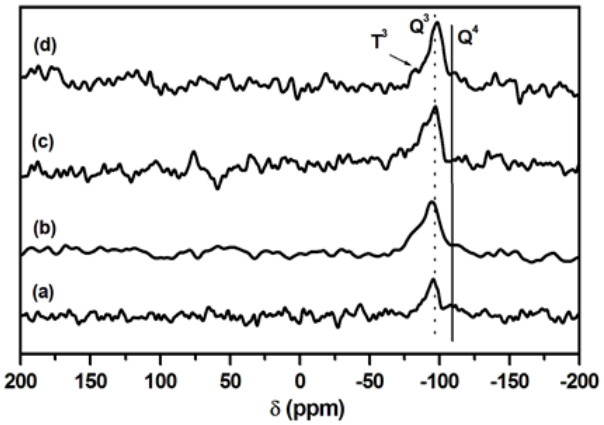

Fig. 5 [29]Si solid state CP/MAS NMR spectra of nanocomposite films: (a) PU-0.5AMS, (b) PU-1AMS, (c) PU-3AMS and (d) PU-5AMS.

3.4 Thermogravimetric studies

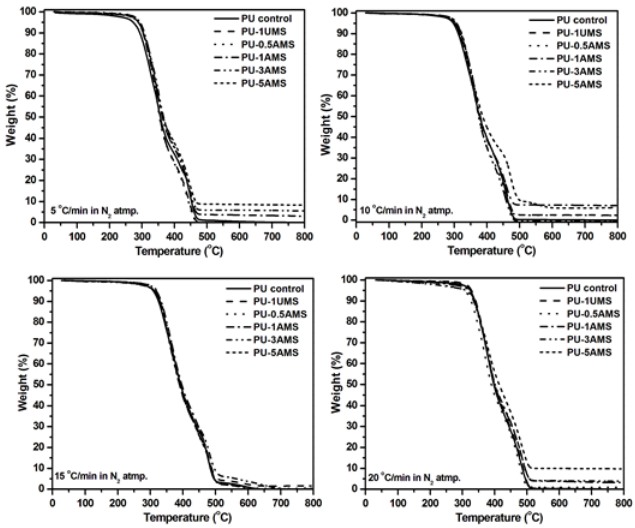

Fig. 6 TGA plots for the polyurethane/silica nanocomposite films taken at different heating rates.

TGA of castor oil based polyurethane/silica nanocomposite films are given in Fig. 6 and their derivative plots given in Fig. S5. Polyurethanes exhibit relatively low thermal stability generally because of the presence of labile urethane bonds and decompose below 250 °C based on the type of isocyanates and polyol used for the synthesis.[34] It can be seen from the thermograms that all the nanocomposite samples start to degrade above 280 °C. The decomposition up to 350 °C may be due to the loss of urethane bonds with the elimination of carbon dioxide.[35] The temperature range between 350 and 500 °C is mainly due to the decomposition of long alkyl chain present in the castor oil moiety. Furthermore, the thermo-oxidative degradation of the polyurethane films takes place above 500 °C. The presence of silica nanoparticle increases the thermal stability of the castor oil polyurethane film and the degradation temperatures for two stages were given in Table S2. The increase in thermal stability behavior clearly seen from the T_5, T_{10} and T_{50} values, where 5, 10 and 50 wt % of the polyurethane film are lost (see Table S3, ESI). The residual weight (%) of the nanocomposite films clearly evidence the improvement in the thermal stability due to the presence of silica nanoparticles. In the case of control polyurethane, the residual weight percentage is 0.003%, whereas, in PU-5AMS is 8.2%. Moreover, the thermal degradation profile shows two-stage degradation and their corresponding temperature maximum (T_{max1} and T_{max2}) values were increased with increasing silica nanoparticle loading.

The activation energy (E_a) parameters for the thermal decomposition process of polyurethane/silica nanocomposite films at two stages were determined by Kissinger method using the following equation:[36,21]

$$\ln\left(\frac{\beta}{T_{max}^{\,2}}\right) = -\frac{E_a}{RT_{max}} + \left\{\ln\frac{AR}{E_a} + \ln\left[n(1-\alpha_{max})^{n-1}\right]\right\} \quad \text{--------- (1)}$$

Where β is the heating rate, T_{max} is the temperature maximum corresponding to the maximum degradation, A is the pre-exponential factor, E_a is the activation energy, α_{max} is the maximum conversion, n is the order of the reaction and R is the universal gas constant. The activation energy can be obtained from the slope (= $-E_a/R$) of linear plot of $\ln(\beta/T_{max}^{\,2})$ vs $1/T_{max}$.

Table 2 Activation energy values for the nanocomposite films.

Codes	1st stage degradation, T_{max1}			2nd stage degradation, T_{max2}		
	Slope	E_a	R^2	Slope	E_a	R^2
PU control	-16064	133	0.992	-16745	139	0.985
PU-1UMS	-16329	136	0.978	-17130	142	0.989
PU-0.5AMS	-16845	140	0.983	-17330	145	0.979
PU-1AMS	-17386	144	0.975	-17791	148	0.992
PU-3AMS	-18109	150	0.992	-19212	159	0.983
PU-5AMS	-18969	157	0.989	-20039	166	0.993

Where E_a in kJ/mol, and R^2 = correlation coefficient.

The calculated activation energy parameters for the nanocomposite films were given in Table 2 and their Kissinger plots depicted in Fig. 7. The E_a values for control polyurethane are 133 and 139 kJ/mol at T_{max1} and T_{max2}, respectively. The activation energy of polyurethane degradation process increased with respect to the concentration of silica nanoparticles. The E_a values for the higher silica content (5 wt %) are 157 and 166 kJ/mol at T_{max1} and T_{max2}, respectively. This clearly proves that the incorporation of silica nanoparticle provides higher thermal stability to the polyurethane films. Furthermore, the weight loss behavior for the nanocomposite films at two different temperatures (350 & 450 °C) at different heating rates also presented in Table S4. The weight loss at 350 and 450 °C also increased with increasing the concentration of the silica nanoparticles. This shows that the incorporation of silica nanoparticle provides good thermal stability due to better interfacial interaction of polyurethane matrix and nanoparticle.[10b] This interfacial interaction provides better reinforcement between SiNPs and polyurethane thereby increasing the degradation temperature and stability of PU matrix.[6b]

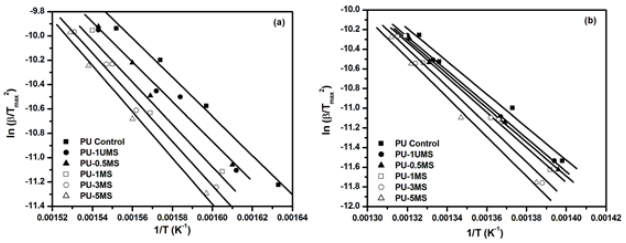

Fig. 7 Kissinger plots for the nanocomposite films at two different stages of the degradation process: (a) Tmax1 and (b) Tmax2.

3.5 Differential scanning calorimetry

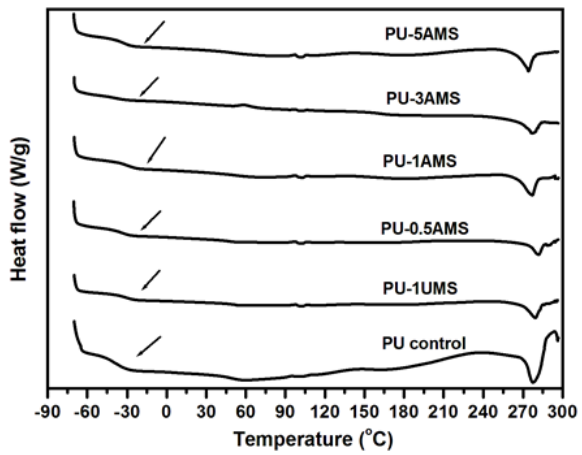

Fig. 8 DSC thermograms for the PU/silica nanocomposite films.

DSC thermograms of castor oil PU and polyurethane/silica nanocomposite films shown in Fig. 8 and their data also given in Table 3. The control castor oil PU shows T_g corresponds to soft segment at -40.1 °C and T_m for the hard segment at 279.1 °C. The glass transition temperature (T_g) values for the silica nanoparticle incorporated polyurethane nanocomposite films were increased with increase in nanoparticle content. The incorporation of silica nanoparticles has significant effect on T_g values of PU, which can be seen from the incremental increase in T_g values (Table 3). This may be due to the presence and well dispersion of silica nanoparticle in the polyurethane matrix, which restricts the molecular motion of PU chains.[37,38] Furthermore, cross-linking present in the nanocomposite also contribute to the increase in T_g.[21] The T_g values for the amine modified silica nanoparticles incorporated nanocomposite films are -33.4, -33.7, -32.6 and -29.7 °C for 0.5, 1, 3 and 5 wt % amine modified silica nanoparticles, respectively. However, the incorporation of silica does not alter much on the T_m values. The melting enthalpy (ΔH) value for the castor oil PU sample is 6.64 J/g, whereas the ΔH values for the amine modified silica nanoparticles incorporated nanocomposite films are 6.8, 11.4, 12.7 and 11.4 J/g for 0.5, 1, 3 and 5 wt % silica nanoparticles, respectively. This shows that the melting enthalpy (ΔH) increased with increasing the fraction of silica nanoparticles up to 3 wt % AMS, which may be due to the presence of strong interfacial interaction between the amorphous silica nanoparticles and hard segment in the polyurethane chain.[39] However, the above ΔH value start to decrease above 3 wt % of AMS. This interfacial interaction restricts the molecular motion of the hard segment in polyurethane.

Table 3 DSC data for PU and PU nanocomposite films.

Codes	Thermal properties		
	T_g (°C)	T_m (°C)	ΔH (J/g) for Tm
PU control	-40.1	279.1	6.6
PU-1UMS	-34.3	279.3	9.1
PU-0.5AMS	-33.4	281.9	6.8
PU-1AMS	-33.7	277.1	11.4
PU-3AMS	-32.6	276.2	12.7
PU-5AMS	-29.7	274.5	11.4

3.6 UV-vis spectra

UV-visible spectra for the polyurethane/silica nanocomposite films were measured to study optical properties and presented in Fig. 9. The control polyurethane film shows good transmittance in the range of 300-800 nm. The peak at 240 nm is the characteristic peak of long alkyl chain with double bond present in castor oil.[40c] In the case of PU nanocomposites, the transmittance decreased with increasing the concentration of silica nanoparticles. The incorporation of silica nanoparticles in the polymer matrix reduces the transmittance of the films. This may be due to the presence of hydrophilic silica nanoparticle, which shields the UV light thereby decreasing the transmittance of the films.[40a] The unmodified silica and amine modified silica nanoparticles give an absorption peaks at around 210 and 220 nm, respectively.[40b] Therefore, UV-vis spectra of nanocomposite show transmittance after 300 nm. This means that SiNPs absorbs UV until 300 nm after that transmit due to this transmittance of polyurethane films decreased with increasing silica concentration. The transmittance at 600 nm decreases from 92% of control polyurethane film to 80% of nanocomposite films with 5 wt % amine modified silica nanoparticle. The decreased optical transmittance of the polyurethane/silica nanocomposite films is likely due to the scattering at the interfaces between the silica nanoparticles and polyurethane.[41]

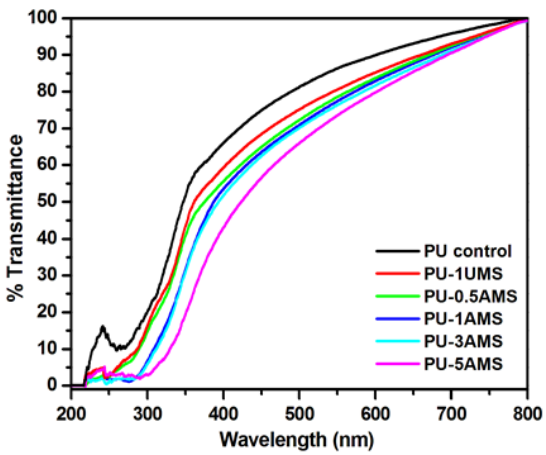

Fig. 9 UV-vis spectra for the polyurethane nanocomposite films.

3.7 XPS spectra

XPS spectra of unmodified and modified silica PU nanocomposites were given in Figs. S6-S9. The XPS is an important tool to investigate about the surface chemistry and composition of the nanocomposite. From the Fig. S6, the peak at

binding energy of 285.5 eV assigned to C_{1s} element present in PU and nanocomposites (PU-0.5AMS, PU-1AMS) were correspond to the C-C bond in the polyurethane structure, which shift the position slightly on disordering with increasing silica nanoparticle.[42] However, the nanocomposites show predominant C_{1s} peak with increased intensity compared to native PU, this might be due to the presence of modified silica nanoparticles, which contain 3-aminopropyl groups on its surface. Along the same line, a small new peak was observed at binding energy of 290.1 eV for nanocomposite samples, which was absent in the native PU. The appearance of a new peak might be due to the physical interaction between the urethane-amide C=O moiety and nanosilica surface.[6c] These findings clearly prove the occurrence of physicochemical interaction between the PU and nano silica in nanocomposites.

The XPS spectra of nitrogen atom give us an important evidence for the interaction of urethane-amide groups in the nanocomposites. The N_{1s} element present in the polyurethane gives a peak at binding energy of 400.7 eV (see Fig. S7, ESI). However, in the case of nanocomposites the peak shifted to higher binding energy of 401.0 eV due to the interaction between amino and amide groups with each other present in the nanoparticle and PU.[43] Similarly, the oxygen (O_{1s}) XPS spectra of polyurethane gives a peak at 533.1 eV corresponds to the -$NHCOO^-$, whereas nanocomposite samples give a strong intense peak at 533.4 eV (see Fig. S8, ESI). This may be due to the overlapping of peaks of Si-O-Si and -$NHCOO^-$ with each other.[44] Furthermore, we also analyzed silica XPS spectra to confirm the presence of nano-silica in PU nanocomposite, which clearly show strong signal of Si_{1s} peak at 103.0 eV (see Fig. S9, ESI). The XPS spectra of nanocomposite clearly show and prove that silica nanoparticles are uniformly dispersed in the PU matrix, and also provide the information about the physicochemical interaction between the nanosilica and the urethane amide moiety of PU. Such interaction helps in improving both mechanical and physical properties of the nanocomposites.

3.8 FE-SEM images of prepared nanocomposites

Field emission scanning electron micrographs of the prepared PU and silica nanocomposite films were given in Fig. 10. In the case of control PU, the fractured surface revealed a homogenous structure due to the cross-linked polyurethane.[45] The PU-1UMS sample also exhibit similar fractured structure like control PU (Fig. 10b), which demonstrates that the UMS did not affect the surface morphology of the nanocomposite film. The introduction of amine modified silica nanoparticles in the PU matrix showed excellent dispersion of silica nanoparticles in the pores of PU matrix, which greatly influenced on the surface of PU. As the concentration of AMS nanoparticles in the PU matrix increased, the sample showed cracked surface initially (PU-0.5AMS) and then the surface turned rough at higher concentration of silica nanoparticles (PU-5AMS), which revealed that the AMS nanoparticles are well dispersed in the lower concentration (Fig. 10d & e) compared to the higher concentration (Fig. 10f). The higher magnification images show embedded SiNPs in PU matrix with difference sizes (images not given).

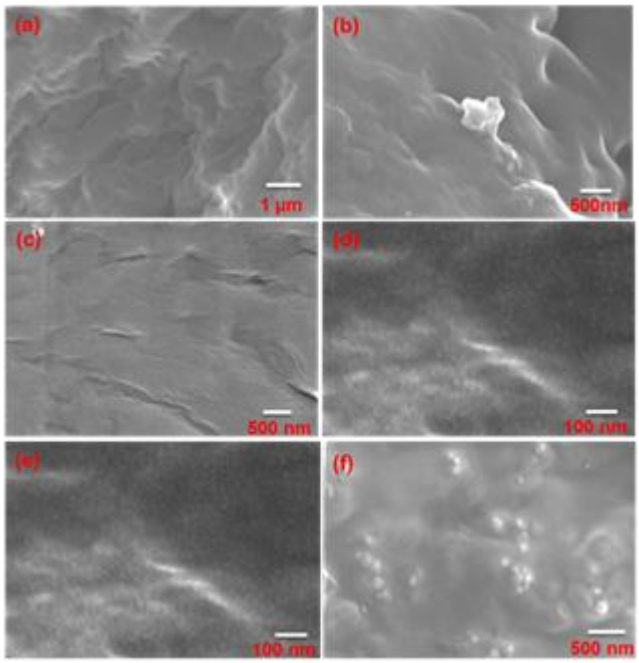

Fig. 10 FE-SEM images of nanocomposite films: (a) PU control (X30K), (b) PU-1UMS (X80K), (c) PU-0.5AMS (X60K), (d) PU-1AMS (X500K), (e) PU-3AMS (X500K) and (f) PU-5AMS (X80K).

3.9 HR-TEM images

The morphology of the silica nanoparticle dispersed in polyurethane was observed by using high resolution transmission electron microscopy and the images were given in Fig. 11. HR-TEM images of polyurethane/silica nanocomposite suggest the presence of nanopores on the surface of polyurethane into which silica nanoparticles were embedded. At low concentration of SiNPs (1 & 3 wt %), the nanoparticles were uniformly dispersed in the polyurethane matrix (Fig. 11a & b), whereas in the case of higher concentration (5 wt %), small aggregates were observed (image not shown here). From HR-TEM images, we observed well defined bright circular spots within which dark circular spots were embedded. These bright circular spots are the pores uniformly distributed on the PU matrix, and the dark circular spots are the silica nanoparticles embedded inside the pores. HR-TEM micrographs provide the evidence of the presence of SiNPs within the pores of polyurethane matrix. Similar kind of morphology was reported for polyamide/silica hybrid nanocomposite by van Zyl *et al.*[46]

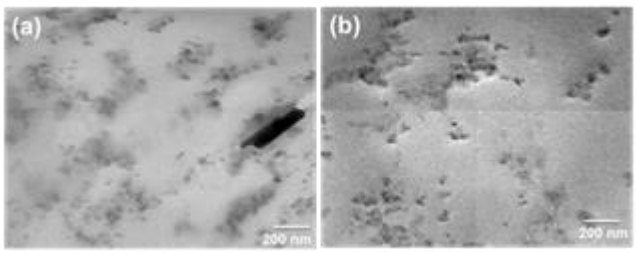

Fig. 11 HR-TEM images of nanocomposites: (a) PU-1AMS, and (b) PU-3AMS.

3.10 Contact angle measurements

Contact angle measurements were obtained for the polyurethane/silica nanocomposites films to calculate their surface free energy and data given in Table 4. The contact angle values of PU/silica nanocomposites film samples were presented in Table 7 and the surface energy was calculated using the following Owens and Wendt equation:[47]

$$\gamma_L (1 + \cos\theta) = 2 (\gamma_S^d \gamma_L^d)^{1/2} + 2 (\gamma_S^p \gamma_L^p)^{1/2} \quad \text{-------- (2)}$$

Where γ_L is the surface tension of the liquids, γ_L^p and γ_L^d are the surface tension of the polar and dispersion components of the liquids, and γ_S^p and γ_S^d are surface tension of the polar and dispersion components of the solids.

Table 4 Contact angle measurements for the PU nanocomposite films.

	Static contact angle (θ, deg)		Surface free energy (mJ/m^2)		
Codes	Water	Hexadecane	γ_s^p	γ_s^d	γ_s^t
PU control	79.3	18.9	6.9	27.3	34.3
PU-1UMS	76.9	Nearly zero	7.6	28.7	36.4
PU-0.5AMS	71.1	”	10.6	28.7	39.4
PU-1AMS	64.1	”	14.7	28.7	43.5
PU-3AMS	50.9	”	23.2	28.7	51.9
PU-5AMS	46.5	9.5	26.7	28.3	55.0

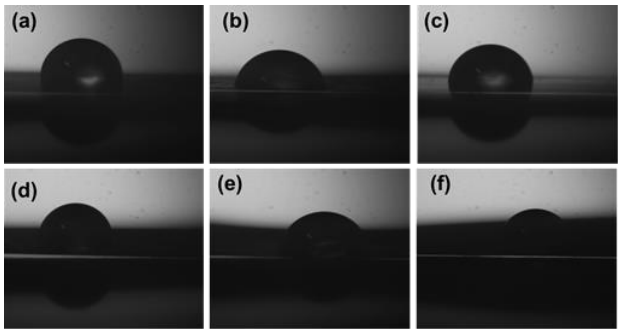

Fig. 12 Water droplets on PU nanocomposite films: (a) PU control, (b) PU-1UMS, (c) PU-0.5AMS, (d) PU-1AMS, (e) PU-3AMS, and (f) PU-5AMS.

The images of water droplets on the surface of polyurethane films were given in Fig. 12. The water contact angle for the PU control film is 79.3º and the corresponding surface energy is 34.3 mJ/m^2. Contact angles of PU/silica nanocomposites film samples decrease with the addition of unmodified silica nanoparticles, which lead to increased surface energy. This is mainly due to the presence of silanol groups on the surface of unmodified silica nanoparticles, which decreased the water contact angle to 76.9º leading towards hydrophilic surface.[48] Further, it is also seen that amine modified silica nanoparticles also give similar kind of behavior i.e. decreased water contact angle. The water contact angles for 0.5, 1, 3 and 5 wt % of amine modified silica nanoparticles were 71.1, 64.1, 50.9 and 46.5°, respectively. Similar kind of trend was also shown in dispersive component. The decrease in contact angle resulted in total surface energy increment. The surface energy for the higher silica (5 wt %) loaded nanocomposite film is 55 mJ/m^2. The incorporation of silica nanoparticle to the polyurethane films imparts wettability to the films. The morphology of nanocomposite also plays an important role in improving surface hydrophilicity and the FE-SEM images clearly shows uniform distribution silica nanoparticle in the polyurethane matrix (Fig. 10d & e). In the case of PU-5AMS, higher silica concentration gives slightly agglomerated structure (Fig. 10f). Further, considering the size of water droplet, the agglomerate size may be neglected and the uniform surface provides hydrophilicity.

3.11 Dynamic mechanical studies

The viscoelastic properties of the castor oil polyurethane/silica nanocomposites were studied from thermo-mechanical properties using DMA. Figs. 13 & 14 show the storage modulus (E') and loss modulus (E") for the nanocomposite films as a function of temperature. The storage modulus values obtained at -50°C and T_g from loss modulus data were presented in Table 5. In Fig. 13, the E' value increased with increasing the silica nanoparticle loading. All the PU samples show increased storage modulus behavior in the glassy region. The storage modulus at -50°C for control polyurethane is 1609 MPa, whereas in the case of 5 wt % amine modified silica nanoparticle incorporated film is 1994 MPa. A large improvement of E' around 24% was obtained due to the presence of SiNPs in the glass transition temperature range. Similar kind of increasing E' value was obtained for the shape memory polyurethane/silica nanocomposite at around T_g by Xu *et al.*[37] The silica nanoparticle provides strong interfacial interaction with polyurethane matrix. This interfacial interaction could transfer the stress from polyurethane to nano silica. Furthermore, silica nanoparticles restrict the mobility of polyurethane chains thereby giving reinforcement to the nanocomposite films.[49] This reinforcement provides the enhancement of E', which indicates that the elastic response is prominent with the increase of nanoparticle loading. Similar kind of behavior was reported by Chang *et al.*[50] for the epoxy resin/silica nanocomposite materials.

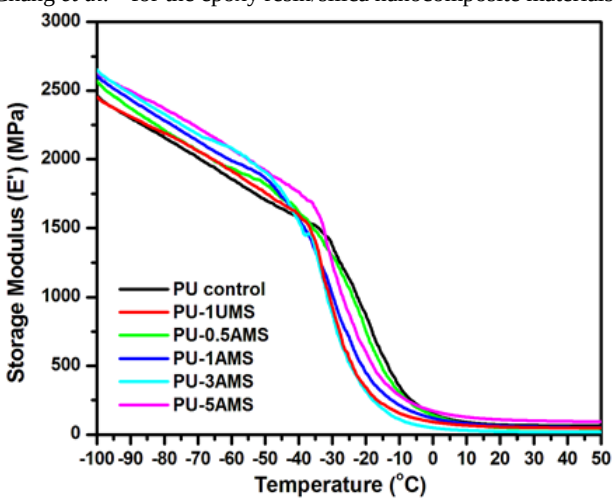

Fig. 13 Storage modulus (E') of PU/silica nanocomposite films.

In Fig. 14, the loss modulus show maximum value in the T_g region and shift towards higher temperature with increasing the silica nanoparticles loading from 0.5 to 5 wt %. It can be seen from the loss modulus graph that E" peak broadening with increasing amount of silica nanoparticles. The T_g value increases from -29.4 to -16.5°C for control polyurethane and PU-5AMS, respectively, which is in good agreement with the DSC results. This may be due to the fact that the presence of nanoparticle

hinders the segmental motion of castor oil polyurethane chain, which resulted from the interfacial interaction and entanglement.[51] The E" graph shows only one peak, which confirms the absence of polymer phase separation. At low temperature, E" value is low due to the frozen state of polymer chains. Upon increasing the temperature, the polymer chain will move freely and reaches a maximum value at T_g.[52]

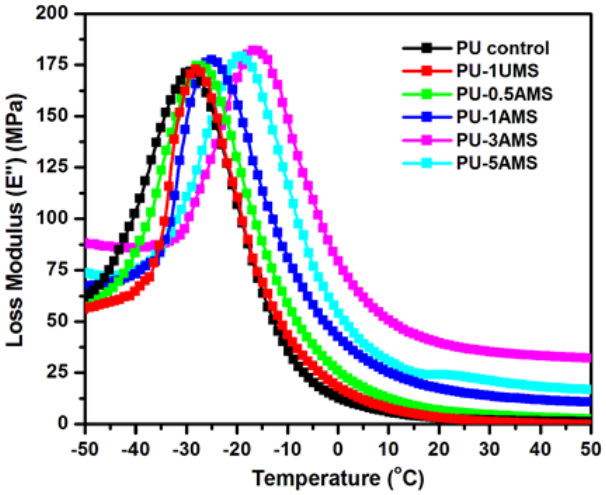

Fig. 14 Loss modulus (E") of PU/silica nanocomposite films.

Table 5 Data of PU/silica nanocomposite films obtained from DMA.

Codes	T_g (°C)[a]	E' (MPa) at -50 °C	% increase
PU control	-29.4	1609	-
PU-1UMS	-28.1	1762	9.5
PU-0.5AMS	-27.6	1823	13.3
PU-1AMS	-24.9	1876	16.6
PU-3AMS	-19.2	1908	18.6
PU-5AMS	-16.5	1994	23.9

[a] obtained from loss modulus graph.

3.12 Tensile Properties

Tensile measurements for the polyurethane/silica nanocomposite films were measured and their stress strain curves presented in Fig. 15. The control polyurethane shows a tensile strength of 3.9 MPa and elongation at break of 67 % (see Table S5, ESI). In the case of nanocomposite film, tensile strength slightly increased from 3.9 to 6.3 MPa for 1 wt % amine modified silica nanoparticle (PU-1AMS) incorporated castor oil polyurethane nanocomposite film. This double enhancement of tensile strength resulted from the interfacial interaction between the nanoparticle and polymer matrix, which transfers load from the polymer matrix to inorganic silica,[53] whereas elongation at break values increased from 67 to 83% in the case of 1 wt % amine modified silica nanoparticle (PU-1AMS) incorporated castor oil PU nanocomposite film with the increase in the cross-link density. Hablot *et al.*[15] reported tensile values of polyurethane films prepared from castor oil with different isocyanates (IPDI, TDI & HDI) in DBTDL catalyst. In comparison with all isocyanates, HDI shows low tensile strength (0.8 MPa) and elongation (31.6%) due to the aliphatic character of HDI. In our system, we got double enhancement of tensile strength upon adding 1 wt % AMS and also considerable improvement in elongation at break value was obtained. The tensile property mainly depends on the compatibility and dispersion of silica nanoparticle in the polyurethane matrix. The ambiguity in the mechanical property of nanocomposite films may be due to the presence of some agglomerates of silica nanoparticles, which may alter the mechanical properties.

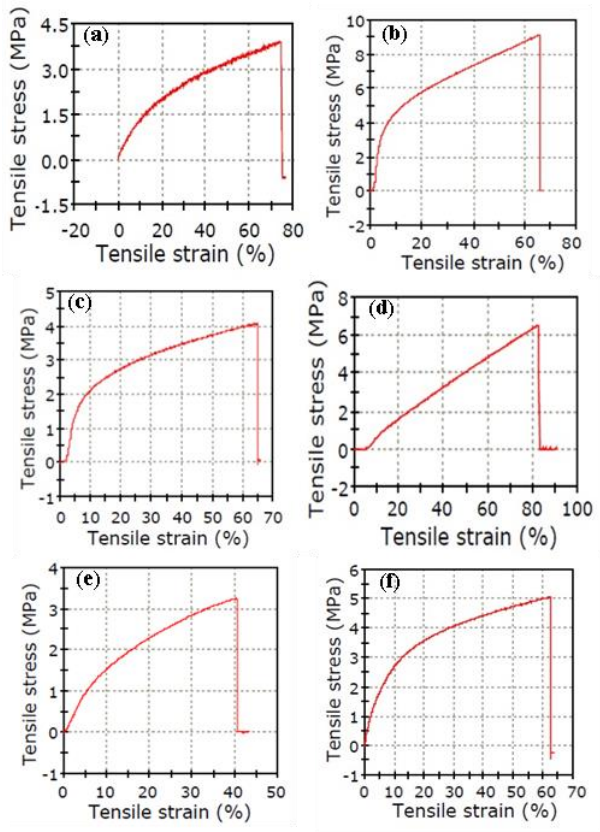

Fig. 15 Stress-strain curves for the prepared PU nanocomposite films: (a) PU control, (b) PU-1UMS, (c) PU-0.5AMS, (d) PU-1AMS, (e) PU-3AMS, and (f) PU-5AMS.

4. Conclusions

Castor oil polyurethanes/silica nanocomposites were prepared through two-step process. In the first step, castor oil polyurethane was made using castor oil and 1,6-hexamethylene diisocyanate in THF at room temperature. In the second step, different concentrations of modified silica nanoparticles were added to the PU solution and cast to obtain films. The surface of the silica nanoparticle was modified with 3-aminopropyltrimethoxysilane coupling agent. ATR-FTIR and Raman spectra confirmed the presence of silica nanoparticle in the PU nanocomposite films. The activation energy for the decomposition of nanocomposite films were calculated using Kissinger method at two different stages (T_{max1} and T_{max2}), which clearly proves the role of SiNPs concentration in improving the thermal stability of the films. Contact angle measurements show that the incorporation of silica nanoparticle decreases the contact angle from 79.3° (PU control) to 46.5° (PU-5AMS), which result in surface energy increment. Overall, silica nanoparticles impart wettability to the PU films. The interfacial interaction between silica and polyurethane increases the tensile strength from 3.9 to 6.3 MPa for PU control and PU-1AMS, respectively. HR-TEM images confirm that SiNPs were present in the pores of polyurethane matrix. Overall,

the results obtained from various physicochemical techniques show that the presence of silica nanoparticle could improve the properties of the polyurethane films, which are useful in the field of biomaterials development.

Acknowledgements

One of the authors (KSM) acknowledges CSIR, India (grant number 31/6(362)/2012-EMR-I) for Senior Research Fellowship. We are grateful to Dr. Tushar Jana and Mr. Sudhangshu Maity, University of Hyderabad, Hyderabad, for permitting and helping us to do DMA measurements. We wish to thank Mr. S. Radhakrishnan, CECRI, Karaikudi, for helping with ^{29}Si solid state NMR analysis. The authors wish to thank the Director, National Centre for Nanoscience & Nanotechnology, University of Madras, Chennai, for HR-TEM and XPS analyses. We thank Dr. Debasis Samantha, CLRI, Chennai, for valuable discussions and Mr. S. Selvakumar, SDSC-SHAR Centre, ISRO, Sriharikota, for helping with GPC analysis.

References

1 (a) A. H. Zou, S. Wu and J. Shen, *Chem. Rev.*, 2008, **108**, 3893-3957; (b) D. G. Papageorgiou, E. Roumeli, K. Chrissafis, Ch. Lioutas, K. Triantafyllidis, D. Bikiaris and A. R. Boccaccini, *Phys. Chem. Chem. Phys.*, 2014, **16**, 4830-4842.

2 (a) S. Stankovich, D. A. Dikin, G. H. B. Dommett, K. M. Kohlhaas, E. J. Zimney, E. A. Stach, R. D. Piner, S. B. T. Nguyen and R. S. Ruoff, *Nature*, 2006, **442**, 282-286; (b) Y. Turhan, M. Dogan and M. Alkan, *Ind. Eng. Chem. Res.*, 2010, **49**, 1503–1513; (b) S. Bai and X. Shen, *RSC Advances*, 2012, **2**, 64–98.

3 (a) J. D. Cho, H. T. Ju and J. W. Hong, *J. Polym. Sci. Part A: Polym. Chem.*, 2005, **43**, 658–670; (b) J. Zeng, Y. Zhou, L. Li and S. P. Jiang, *Phys. Chem. Chem. Phys.*, 2011, **13**, 10249–10257.

4 (a) Y. Xia and R. C. Larock, *Macromol. Rapid Commun.*, 2011, **32**, 1331-1337; (b) K. M. Seeni Meera, R. Murali Sankar, A. Murali, S. N. Jaisankar and A. B. Mandal, *Colloids Surf., B*, 2012, **90**, 204–210.

5 (a) S. Ghosh, A. Sannigrahi, S. Maity and T. Jana, *J. Phys. Chem. C*, 2011, 115, 11474–11483; (b) W. C. Wang, J. J. Lin, H. J. Tseng and S. H. Hsu, *ACS Appl. Mater. Interfaces*, 2012, **4**, 338−350.S. N. Jaisankar, S. Ramalingam, H. Subramani, R. Mohan, P. Saravanan, D. Samanta and A. B. Mandal, *Ind. Eng. Chem. Res.*, 2013, **52**, 1379−1387.

6 (a) S. Srinivasan, V. K. Praveen, R. Philip and A. Ajayaghosh, *Angew. Chem. Int. Ed.*, 2008, **47**, 5750–5754; (b) Z. Luo, R.Y. Hong, H. D. Xie, W. G. Feng, *Powder Technol.*, 2012, **218**, 23-30; (c) R. Murali Sankar, K. Seeni Meera, A. B. Mandal and S. N. Jaisankar, *High Perform. Polym.*, 2013, **25**, 135–146.

7 (a) M. Hazarika and T. Jana, *Compos. Sci. Technol.*, 2013, **87**, 94-102; (b) J. T-W. Wang, J. M. Ball, E. M. Barea, A. Abate, J. A. Alexander-Webber, J. Huang, M. Saliba, I. Mora-Sero, J. Bisquert, H. J. Snaith and R. J. Nicholas, *Nano Lett.*, 2014, **14**, 724-730.

8 (a) S. Ghosh, S. Maity and T. Jana, *J. Mater. Chem.*, 2011, **21**, 14897 14906; (b) R. K. Donato, K. Z. Donato, H. S. Schrekker and L. Matejka, *J. Mater. Chem.*, 2012, **22**, 9939–9948.

9 (a) S. Jain, H. Goossens, F. Picchioni, P. Magusin, B. Mezari and M. van Duin, *Polymer*, 2005, **46**, 6666–6681; (b) M. Edrissi, M. Soleymani and M. Adinehnia, *Chem. Eng. Technol.*, 2011, **34**, 1813–1819.

10 (a) K. M. S. Meera, R. M. Sankar, S. N. Jaisankar and A. B. Mandal, *Colloids Surf., B* 2011, **86**, 292–297; (b) I. A. Rahman and V. Padavettan, *J. Nanomater.*, 2012, **2012**, 1-15.

11 L. Wang, J. Li, R. Hong and H. Li, *In Polymer Composites:* Nanocomposites, eds. S. Thomas, K. Joseph and S. K. Malhotra, Wiley-VCH Verlag GmbH & Co. KGaA: Germany, 2013; Vol. 2, p 19.

12 (a) H. T. Jeon, M. K. Jang, B. K. Kim and K. H. Kim, *Colloids Surf., A*, 2007, **302**, 559–567; (b) K. C. Pradhan and P. L. Nayak, *Adv. Appl. Sci. Res.*, 2012, **3**, 3045-3052.

13 (a) S. N. Jaisankar, D. J. Nelson and C. N. Brammer, *Polymer*, 2009, **50**, 4775–4780; (b) A. Palanisamy, *Polym Compos.*, 2013, **34**, 1306-1312.

14 (a) J. Xiong, Y. Liu, X. Yang, X. Wang, *Polym. Degrad. Stab.*, 2004, **86**, 549–555; (b) S. Chen, Q. Wang and T. Wang, *Mater. Chem. Phys.*, 2011, **130**, 680-684.

15 (a) E. Hablot, D. Zheng, M. Bouquey and L. Averous, *Macromol. Mater. Eng.*, 2008, **293**, 922–929; (b) S. Tan, T. Abraham, D. Ference, C. W. Macosko, *Polymer*, 2011, **52**, 2840-2846.

16 (a) Z. Wu, H. Wang, X-Y. Tian, P. Cui, X. Ding and X. Ye, *Phys. Chem. Chem. Phys.*, 2014, DOI: 10.1039/C3CP54429J; (b) A. Mishra, B. P. D. Purkayastha, J. K. Roy, V. K. Aswal, P. Maiti, *J. Phys. Chem. C*, 2012, **116**, 2260–2270.

17 (a) S. A. Gurusamy-Thangavelu, S. J. Emond, A. Kulshrestha, M. A. Hillmyer, C. W. Macosko, W. B. Tolman and T. R. Hoye, *Polym. Chem.* 2012, **3**, 2941−2948; (b) R. L. Quirino and T. F. Garrison, M. R. Kessler, *Green Chem.*, 2014, DOI: 10.1039/C3GC41811A

18 (a) B. R. Babu, K. S. Meera, P. Venkatesan and D. Sunandha, *Water Air Soil Pollut.*, 2010, **211**, 203–210; (b) C. Zhang, Y. Xia, R. Chen, S. Huh, P. A. Johnston and M. R. Kessler, *Green Chem.*, 2013, **15**, 1477-1484.

19 (a) Y. Xia and R. C. Larock, *Green Chem.*, 2010, **12**, 1893-1909; (b) M. L. Robertson, J. M. Paxton and M. A. Hillmyer, *ACS Appl. Mater. Interfaces*, 2011, **3**, 3402–3410; (c) S. Thakur and N. Karak, *RSC Adv.*, 2013, **3**, 9476-9482.

20 (a) P. Florian, K. K. Jena, S. Allauddin, R. Narayan and K. V. S. N. Raju, *Ind. Eng. Chem. Res.*, 2010, **49**, 4517-4527; (b) I. S. Ristic, J. Budinski-Simendic, I. Krakovsky, H. Valentova, R. Radicevic, S. Cakic and N. Nikolic, *Mater. Chem. Phys.*, 2012, **132**, 74–81; (c) B. De, K. Gupta, M. Mandal and N. Karak, *ACS Sustainable Chem. Eng.*, 2014, DOI: 10.1021/sc400358b.

21 K. M. Seeni Meera, R. Murali Sankar, S. N. Jaisankar and A. B. Mandal, *J. Phys. Chem. B*, 2013, **117**, 2682−2694.

22 (a) F. Yucedag, C. Atalay-Oral, S. Erkal, A. Sirkecioglu, D. Karasartova, F. Sahin, S. B. Tantekin-Ersolmaz and F. S. Guner, *J. Appl. Polym. Sci.*, 2010, **115**, 1347–1357; (b) A. Yari, H. Yeganeh, H. Bakhshi and R. Gharibi, *J. Biomed. Mater. Res., Part A*, 2014, **102**, 84-96.

23 E. Sharmin, D. Akram, A. Ghosal, O. Rahman, F. Zafar and S. Ahmad, *Prog. Org. Coat.*, 2011, **72**, 469–472.

24 (a) S. Allauddin, R. Narayan and K. V. S. N. Raju, *ACS Sustainable Chem. Eng.*, 2013, **1**, 910–918; (b) A. Shaik, R. Narayan and K. V. S. N. Raju, *J. Coat. Technol. Res.*, 2014, DOI: 10.1007/s11998-013-9548-5.

25 Z. K. Wang, D. Wang, H. Wang, J. J. Yan, Y. Z. You and Z. G. Wang, *J. Mater. Chem.*, 2011, **21**, 15950–15956.

26 H-S. Jung, D-S. Moon and J-K. Lee, *J. Nanomater.*, 2012**, 2012**, 1–8.

27 (a) D. Liu, H. Tian, L. Zhang and P. R. Chang, *Ind. Eng. Chem. Res.*, 2008, **47**, 9330–9336; (b) X. Ji, Y. Zhou, B. Zhang, C. Hou and G. Ma, *ISRN Polym. Sci.*, 2013, **2013**, 1-10.

28 (a) A. K. Mishra, D. K. Chattopadhyay, B. Sreedhar and K. V. S. N. Raju, *Prog. Org. Coat.* 2006**, 55**, 231−243; (b) H. H. Wang, J. Mou, Y. H. Ni, G. Q. Fei, C. L. Si, J. Zou, *eXPRESS Polym. Lett.*, 2013, **7**, 443-455.

29 V. Romanova, V. Begishev, V. Karmanov, A. Kondyurin and M. F. Maitz, *J. Raman Spectrosc.* 2002, **33**, 769–777.

30 S. Parnell, K. Min and M. Cakmak. *Polymer*, 2003, **44**, 5137–5144.

31 D. Fischer, D. Pospiech, U. Scheler, R. Navarro, M. Messori and P. Fabbri, *Macromol. Symp.*, 2008, **265**, 134–143.

32 C-H. Yang, F-J. Liu, L-P. Liu and W-T. Liao, *J. Colloid Interface Sci.*, 2006, **302**, 123–132.

33 D. Wencel, M. Barczak, P. Borowski and C. McDonagh, *J. Mater. Chem.* 2012, **22**, 11720–11729.

34 X. Ying, C. L. Richard, *Macromol. Rapid Commun.*, 2011, **32**, 1331-1337.

35 Z. S. Petrovic, L. Yang, A. Zlatanic, W. Zhang and I. Javni, *J. Appl. Polym. Sci.*, 2007, **105**, 2717–2727.

36 J. Li, L. F. Tong, Z. P. Fang, A. J. Gu and Z. B. Xu, *Polym. Degrad. Stab.*, 2006, **91**, 2046–2052.

37 L. Xu, Y. Fu and M. Du, *Chin. J. Chem.*, 2011, **29**, 703–710.
38 J-Z. Ma, J. Hu and Z-J. Zhang, *Eur. Polym. J.*, 2007, **43**, 4169–4177.
39 S.-I. Lee, Y. B. Hahn, K. S. Nahm and Y.-S. Lee, *Polym. Adv. Technol.*, 2005, **16**, 328–331.
40 (a) S-X. Zhou, L-M. Wu, J. Sun and W-D. Shen, *J. Appl. Polym. Sci.*, 2003, **88**, 189–193; (b) T. Amirthalingam, J. Kalirajan and A. Chockalingam, *J. Nanomedic. Nanotechnol.*, 2011, **2**, 1-5; (c) K. A. Kumar and K. Viswanathan, *J. Spectrosc.*, 2013, **2013**, 1-5.
41 W. C. Lin, C. H. Yang, T. L. Wang, Y. T. Shieh and W. J. Chen, *eXPRESS Polym. Lett.*, 2012, **6**, 2–13.
42 J. T. Park, J. A. Seo, S. H. Ahn, J. H. Kim and S. W. Kang, *J. Ind. Eng. Chem.* **2010**, **16**, 517–522.
43 Y. An, M. Chen, Q. Xue and W. Liu, *J. Colloid Interface Sci.*, 2007, **311**, 507–513.
44 L. Zhai, R. Liu, F. Peng, Y. Zhang, K. Zhong, J. Yuan and Y. Lan, *J. Appl. Polym. Sci.*, 2013, **128**, 1715–1724.
45 Z. Gao, J. Peng, T. Zhong, J. Sun, X. Wang and C. Yue, *Carbohydr. Polym.*, 2012, **87**, 2068–2075.
46 W. E. van Zyl, M. Garcia, B. A. G. Schrauwen, B. J. Kooi, J. T. M. d. Hosson and H. Verweij, *Macromol. Mater. Eng.*, 2002, **287**, 106–110.
47 D. K. Owens and R. C. Wendt, *J. Appl. Polym. Sci.*, 1969, **13**, 1741–1747.
48 A. Valles-Lluch, G. G. Ferrer and M. M. Pradas, *Eur. Polym. J.*, 2010, **46**, 910–917.
49 H. Gu, J. Guo, Q. He, S. Tadakamalla, X. Zhang, X. Yan, Y. Huang, H. A. Colorado, S. Wei and Z. Guo, *Ind. Eng. Chem. Res.*, 2013, **52**, 7718−7728.
50 K-C. Chang, C-Y. Lin, H-F. Lin, S-C. Chiou, W-C. Huang, J-M. Yeh and J-C. Yang, *J. Appl. Polym. Sci.* 2008, **108**, 1629–1635.
51 C. Zhang, W. W. Tjiu, T. Liu, W. Y. Lui, I. Y. Phang and W-D. Zhang, *J. Phys. Chem. B*, 2011, **115**, 3392–3399.
52 S. Chen, Q. Wang, X. Pei and T. Wang, *J. Appl. Polym. Sci.*, 2010, **118**, 1144–1151.
53 S. Zhang, RenLiu, J. Q. Jiang, C. Yang, M. Chen and X. Liu, *Prog. Org. Coat.*, 2011, **70**, 1–8.